UCLA
UCLA Previously Published Works

Title
Exchange Reactions between Alkanethiolates and Alkaneselenols on Au{111}

Permalink
https://escholarship.org/uc/item/2vw2525r

Journal
Journal of the American Chemical Society, 136(22)

ISSN
0002-7863

Authors
Hohman, J Nathan
Thomas, John C
Zhao, Yuxi
et al.

Publication Date
2014-06-04

DOI
10.1021/ja503432f

Peer reviewed

Exchange Reactions between Alkanethiolates and Alkaneselenols on Au{111}

J. Nathan Hohman,*[,†] John C. Thomas,[†] Yuxi Zhao,[†] Harsharn Auluck,[†] Moonhee Kim,[†] Wouter Vijselaar,[‡] Sander Kommeren,[‡] Andreas Terfort,*[,§] and Paul S. Weiss*[,†,‖]

[†]California NanoSystems Institute and Department of Chemistry and Biochemistry, University of California, Los Angeles, California 90095, United States

[‡]Department of Science and Technology, University of Twente, P.O. Box 217, 7500 AE Enschede, The Netherlands

[§]Institut für Anorganische und Analytische Chemie, Universität Frankfurt, Frankfurt 60438, Germany

[‖]Department of Materials Science and Engineering, University of California, Los Angeles, California 90095, United States

S *Supporting Information*

ABSTRACT: When alkanethiolate self-assembled monolayers on Au{111} are exchanged with alkaneselenols from solution, replacement of thiolates by selenols is rapid and complete, and is well described by perimeter-dependent island growth kinetics. The monolayer structures change as selenolate coverage increases, from being epitaxial and consistent with the initial thiolate structure to being characteristic of selenolate monolayer structures. At room temperature and at positive sample bias in scanning tunneling microscopy, the selenolate−gold attachment is labile, and molecules exchange positions with neighboring thiolates. The scanning tunneling microscope probe can be used to induce these place-exchange reactions.
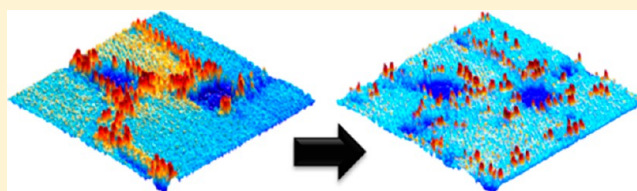
INTRODUCTION

Self-assembled monolayers (SAMs) are test beds for two-dimensional (2D) assembly and control. Despite 30 years of study and myriad applications, the well-known covalent gold−sulfur bond between alkanethiol and the gold surface remains poorly understood. A confluence of studies employing such methodologies as scanning probe microscopy, X-ray diffraction, computation, and others now support the generally accepted model of a sulfur−gold adatom complex.[1−6] Consensus has emerged that this energetically stable gold adatom complex exists, which has sulfur atoms bound to gold atoms or on opposite sides of the gold adatom in a barbell config-uration.[2−4,6−15] We have observed the important roles of gold adatoms in motion of gold−thiolate complexes[1] and in conformational changes of molecular switches.[16] Assuming the existence of an adatom complex, critical unresolved questions remain. Is the adatom layer ordered or disordered, or can it transition from one to the other? Are gold adatoms derived from the initial lift of the herringbone reconstruction,[17−19] or are they abstracted from the unreconstructed surface, leaving behind vacancy sites?[5,7] What is the significance of a proposed barbell motif relative to other binding models in the context of molecular-exchange and place-exchange reactions?[20−25] To-ward answering such questions, we have explored exchange reactions between alkaneselenols and alkanethiolate mono-layers. The exchange reaction of an alkaneselenol molecule into a preformed alkanethiolate SAM occurs at a substrate presenting nominally complete gold−thiolate complex cover-age. We investigate the products of this reaction in the context

of a mobile, labile adatom complex. The Au{111} herringbone reconstruction[17] is already lifted by thiolate deposition, so Au−S/Se exchange reactions provide an opportunity to examine reaction products in the context of the gold adatom complex.[1]

Replacing thiols with selenols has attracted interest for improving the overall oxidative and thermal stability of SAMs, and (in some cases) the electronic coupling of molecules to the substrate.[26−37] Selenium tends to out-compete sulfur for binding sites on the gold substrate.[38,39] Studies of likely binding sites for the selenium atoms are in their relative infancy, with models not yet taking into account discoveries in the chemistry of sulfur−gold adatom complexes. Of primary interest is the configuration of the selenolate attachment: by observing coexisting structures of the two chalcogenolates, we may obtain insight into whether selenium is attached to the substrate in a manner similar to the attachment of sulfur.

In this article, we compare and contrast the structures formed by single-component alkanethiolate and alkaneselenolate films on Au{111}, and then report the structures formed by and the kinetics of the rapid molecular-exchange reaction between gold-bound alkanethiolates and alkaneselenols.

Additionally, we observe 2D place-exchange reactions between adsorbed thiolates and selenolates induced by a scanning tunneling microscope (STM) tip. This chemical system provides a basis for investigating both gold−thiolate and gold−selenolate attachment chemistry. Our observations
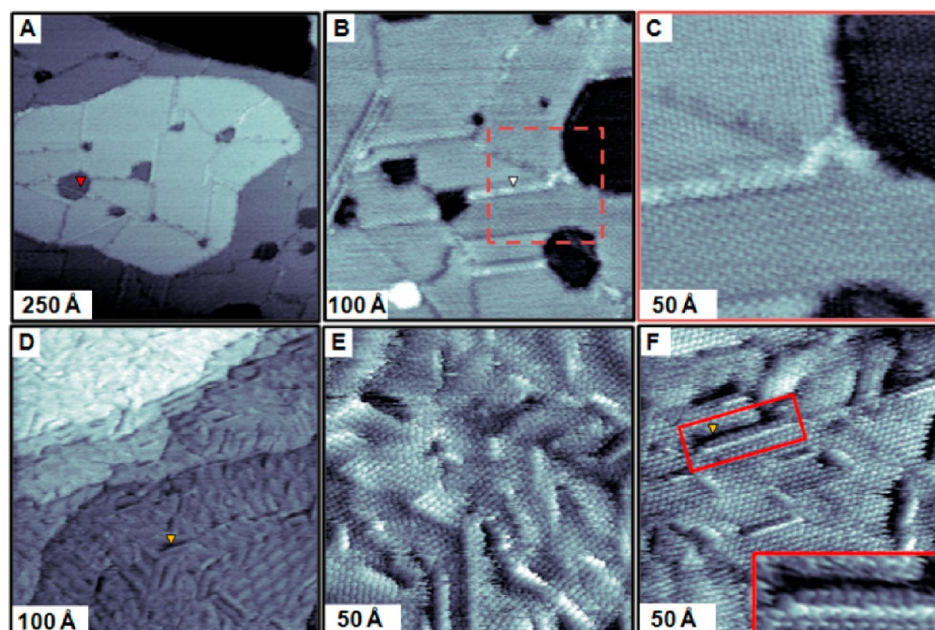
Figure 1. Comparison of scanning tunneling microscope images of single-component 1-decanethiolate (C10, top) and 1-dodecaneselenolate (C12Se, bottom) self-assembled monolayers (SAMs) on Au{111} obtained at a tunneling current of 3 pA and a sample bias voltage of −1 V. (A−C) The annealed C10 monolayer is highly ordered, with large domains. Images A and B shows important defect sites, including roughly circular vacancy island substrate defects (A, red arrow) and linear domain boundaries SAM defects (B, white arrow) that appear either more or less protruding than the surrounding lattice. Panel C shows a high-resolution image of the enclosed region in B. (D−F) The C12Se monolayer is ordered locally, but shows local variations in apparent height. The periodicity of the variation gives rise to the apparent Moiré pattern visible in the lower right section of image D.[26] The features align with the underlying substrate, with linear features rotated with respect to one another in integer multiples of 30°. Panel F shows vacancy islands in single-component C12Se SAMs, hereafter described as vacancy trenches, presenting as narrow, linear depressions aligned with the close-packed direction of the substrate (examples denoted with yellow arrows in images D and F). Vacancy trenches are often accompanied by a pair of C12Se molecular rows, which appear to be depressed or protruding from the median terrace height by −1 or +1 Å, respectively. The inset in panel F shows an expanded view of the region bounded by the red box. The median trench apparent height is ∼2.3 Å lower than the median terrace apparent height, reflecting a monatomic step of the gold substrate surface.

suggest that, initially, the gold−selenolate structure occupies the same binding structure and configuration as the gold−thiolate complex, but as selenolate coverage increases, there is a transition to a new interface structure.

RESULTS AND DISCUSSION

Morphological Comparisons of Alkanethiolate and Alkaneselenolate Monolayer Structures. The STM is capable of exquisite molecular- and atomic-scale resolution, but does not intrinsically provide a means for chemical identification beyond the relative sizes and conductance of the molecules measured.[40−42] To investigate alkanethiolates and alkaneselenolates in mixed, ordered systems, we chose to employ different alkyl chain lengths for the two species: a shorter alkyl chain for the 1-decanethiolate (C10) matrix, and a slightly longer 1-dodecaneselenolate (C12Se). The difference in height enables the identification of the two molecular species at various stages of their exchange reaction.[27,43] Figure 1 details a morphological comparison of single-component C10 and C12Se SAMs on Au{111}.

Imaging an annealed C10 SAM (Figure 1A−C) reveals the expected well-ordered hexagonal lattice of molecules in the $(\sqrt{3}\times\sqrt{3})R30°$ configuration. There are two important classes of defects: domain boundaries and gold substrate step-edges (of which the circular depressions in Figure 1A, substrate vacancy islands, are a subclass).[36,44−47] Ordered molecular domains having different alkyl chain azimuthal orientations are typically separated by domain boundaries.[46,48−50] Domain boundaries

appear either more or less protruding than the surrounding domains, depending on the configuration of molecules at that interface.[46] In highly ordered films, such as the annealed film shown in Figure 1A−C, domain boundaries tend to align with the close-packed substrate lattice directions, with different boundaries oriented 60° with respect to one another. Molecular vacancies are defined as one or more molecules missing from an otherwise well-ordered lattice, a rare monolayer defect in well-ordered alkanethiolate films. Substrate step-edges are a single gold atom high transition from one atomically flat terrace to the next. Gold terrace step-edges and the step-edges at substrate vacancy islands are functionally identical in structure and behavior.

The C12Se films[26,27,51] are strikingly dissimilar from the alkanethiolate films, as reported previously, despite the identical geometries of the alkyl chains (Figure 1D,E). Absent are the characteristic alkanethiolate domain boundary structures,[46,52] such as those observed in the C10 SAM images. Instead, the Moiré patterns of topographic differences are readily apparent in the STM images of the C12Se film (Figure 1D). These patterns originate from differences in the lattice constants of the gold substrate and the overlying molecular layer and result in a smooth, continuous variation of molecular apparent height by ∼1 Å. These features generally align with the substrate, rotated with respect to one another by multiples of 30°, as seen previously in annealed monolayers of 1-adamantaneselenolate.[32]

The substrate step-edges tend to align along the close-packed directions of the gold substrate after C12Se adsorption.
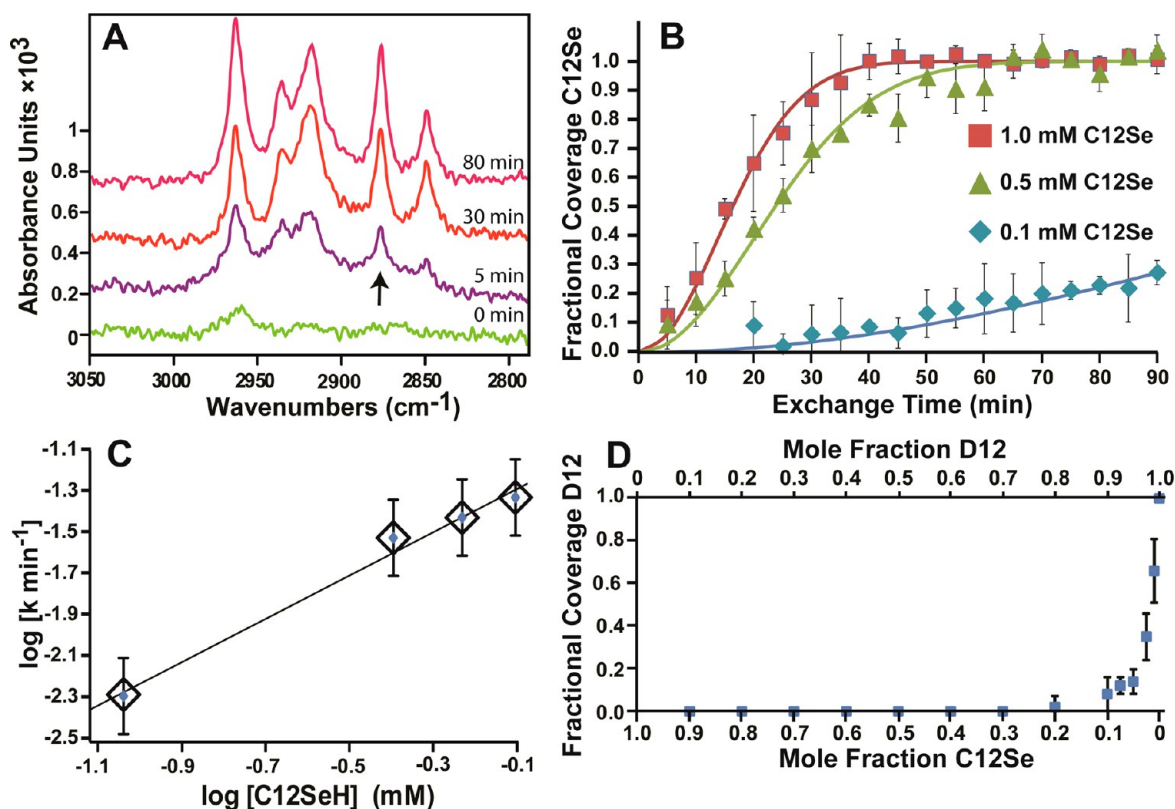
Figure 2. Tracking the exchange of perdeuterated 1-dodecanethiol (D12) by 1-dodecaneselenol (C12Se) via infrared reflectance absorption spectroscopy. (A) Spectral evolution of the C12Se spectrum as it displaces the D12 film. Spectral interference over the shown range was eliminated by employing the deuterated species. The coverage indicator is the 2877 cm^{-1} methyl symmetric stretch, denoted by the black arrow. After 90 min, the reaction has reached completion, and no further exchange occurs. (B) Examples of kinetic experiments tracking the progression of the exchange reaction between a preformed D12 film and C12Se in solution. The data are fit to a site-saturated JMAK2 model for perimeter-dependent island growth.[57] (C) Plotting rate constant of displacement versus C12Se concentration on a logarithmic scale gives a slope of ~1, implying that the rate constant is directly proportional to the concentration of C12Se. (D) Co-deposition studies of D12 with C12Se demonstrating the preference for C12Se in mixed monolayers. C12Se dominates the coverage of a film until the mole fraction approaches 100:1 in favor of D12.

Additionally, high-resolution STM imaging enables us to report the presence of narrow "vacancy trenches" in the single-component C12Se SAMs. These configurations are consistent structurally with the round vacancy islands found in C12 SAMs. Each trench shows a median apparent height that is ~2.3 Å lower than the median apparent height of the surrounding terrace, indicative of a gold substrate monatomic step. The trenches tend to elongate along the crystallographic close-packed direction of the gold substrate. The missing row of the vacancy trench is often accompanied by parallel C12Se molecular rows that are dissimilar from the surrounding lattice. A typical image at high resolution is shown in Figure 1F. The row adjacent to the trench is less protruding than the median height of the surrounding terrace, while the next row is more protruding by the same value of 1 Å. These features highlight the variability of bonding configurations available for the Au–Se interactions, depending on the immediate local environment.

The C12Se SAM structure reflects the underlying crystallographic structure of the gold substrate, and the differences in apparent height of various features imply several binding configurations coexisting with the gold substrate, a feature we previously reported in our study of the 1-adamantaneselenolate system on Au{111}.[32] From our observations, we can confirm that the C12Se SAM formation lifts the gold herringbone reconstruction and spawns vacancy islands. Additionally, the

selenolate–gold interaction results in straightened substrate step-edge features, and produces only small vacancy trenches (compared to the large vacancy islands produced after alkanethiolate deposition). The straightening and existence of multiple binding sites are consistent both with our previous suggestions of gold–selenolate bond promiscuity,[26,27] and with more recent examples suggesting a number of acceptable binding configurations for selenium to gold.[32,53] Rapid straightening of gold substrate features also suggests that the gold–selenolate complex is more mobile than its sulfur counterpart. We will return to discuss the mobility of the selenolate and the hypothesized gold–selenolate complex below.

Molecular-Exchange and Place-Exchange Reactions of Self-Assembled Monolayers. We will now introduce and define terms that are important for understanding the phenomena and associated time scales of reactions that occur between molecules in SAMs. There are two distinct types of exchange reactions described in this article. These two reactions are related, but are treated separately here. First, we define a molecular-exchange (or displacement) reaction as the replacement of an adsorbed molecule by a second species, typically accomplished by immersion of a preformed SAM-coated substrate into a solution or vapor of the replacing chemical.[54–56] The term "insertion" refers to the initial stage of a molecular-exchange reaction, where molecules of the

second species can be found decorating the defect sites of the preformed film.[54,57] Such sites are well known to provide access to the substrate for other species and for chemical reactions,[24,26,45,48,56,58−67] and are the first to be occupied. Defects are critical to both insertion and displacement.

Second, we define a place-exchange reaction as a position exchange between proximate molecules in a 2D lattice, without desorption of either molecule. For our investigations of place-exchange reactions, C12Se is incorporated into the C10 SAM by a molecular-exchange reaction that is arrested before a large fraction of the initial monolayer is displaced. Place-exchange reactions are mediated by defects.[22,68]

Exchange between adsorbed molecular assemblies and molecules in solution is mediated by four primary factors: the chemistry of the molecule/substrate attachment, molecular geometries, intermolecular forces, and the type and density of defects (of both the supramolecular assembly and the substrate, i.e., by access to the substrate). In the case of molecular self-exchange (e.g., the exchange between a 1-dodecanethiolate monolayer and 1-dodecanethiol, C12), most molecules are kinetically trapped in domains, and exchange occurs primarily at defect sites.[20] The constituent molecules can be tailored to engineer molecular-exchange reactions. For instance, a combination of weak intermolecular interactions and low surface density makes 1-adamantanethiolate SAMs susceptible to molecular exchange by *n*-alkanethiols.[54,57,69] Also, monolayer defects and disorder can be induced by exothermic reactions.[70,71] The attachment chemistry also plays an important role. Selenols have previously been shown to out-compete sulfur for binding sites on Au{111}. Packing densities of C12 and C12Se are similar,[26,72] so a thermodynamic drive toward increased coverage is absent.[57] The Se−Au bond is stronger than the S−Au bond;[73] we have shown that the Se−Au bond is more promiscuous in terms of binding sites.[26] Garrell and co-workers[38] showed a strong surface preference for benzeneselenolates over benzenethiolates, a phenomenon attributed to the higher acidity of the selenol group relative to the thiol. Similar experiments on copper-supported monolayers of thiolates and selenolates did not show strong preferences for either chalcogen.[74,75] Substrates can also be engineered to promote exchange.[76,77]

Place exchange between adsorbed thiolates is generally slow in full-coverage monolayers.[20,21,24,57,78−80] Most monolayer dynamics within crystalline domains of nearly complete SAMs occur over short distances and over time scales of hours or longer. There is a notable difference at defect sites, where dynamics are relatively fast, but there is little precedent for covalently bound molecules to transit long distances.[59] We have previously observed apparent site-hopping of adamantaneselenolates on Au{111}, although these motions are thought to occur between adjacent sites separated by only a few angstroms.[32] The even greater promiscuity of amine−Au bonds might be expected to lead to enhanced mobility of these species.[81]

Determination of Exchange Kinetics by Infrared Spectroscopy. We employ infrared reflectance absorption spectroscopy (IRRAS) to measure the kinetics of SAM exchange/displacement. This method has several advantages for tracking changes in monolayers: gold reflectivity is high, the carbon−hydrogen bonds absorb strongly between 2800 and 3000 cm^{-1}, coverage down to a few percent of a monolayer can be detected, and the resulting spectra provide both coverage and structural information.

A typical spectrum for a C12Se SAM, shown as the top spectrum in Figure 2A, is analogous to that of most alkanethiolates on gold. There are five dominant spectral features: methylene symmetric and asymmetric stretches at 2850 and 2918 cm^{-1}, respectively, methyl symmetric and asymmetric stretches at 2877 and 2963 cm^{-1}, respectively, and a weak band associated with a Fermi resonance of the symmetric methyl stretch with a methyl deformation mode, presented as a shoulder of the methylene asymmetric stretch.[82−84] The intensity and position of the methylene asymmetric stretch correlate to monolayer order. The peak position at 2919 cm^{-1} is consistent with a highly ordered, solid-like film. The intensity of the methylene symmetric stretch relative to the other peaks is lower than those reported for selenolate monolayers deposited from dialkyldiselenide.[72] We note that the microscopic structure we have observed for monolayers fabricated from alkaneselenol appears topographically dissimilar to monolayers deposited from dialkyl diselenide (a surface that has been reported to show a substantially larger number of gold substrate defects as compared to our observations for alkaneselenol films).[85] A thorough comparison of alkaneselenol versus dialkyl diselenide self-assembly characterization is warranted.

For determining partial coverage of alkanethiolate monolayers, the methyl symmetric stretch (2877 cm^{-1}) is an important spectral feature; taking the ratio of the peak area at each time point to the peak area after 24 h displacement yields fractional coverage. The symmetry of the group gives it a largely uniform intensity over a range of possible standing-up configurations, making it a useful metric for coverage in mixed systems of standing-up phase alkanethiolate SAMs.[57,84] In the case of C10 exchange by C12Se, the intensity of the 2877 cm^{-1} peak is nominally constant throughout the experiment, as the overall coverage and orientation of the terminal methyl groups remain static. Spectral interference is too high for accurate observation of the exchange reaction, and monitoring intensity changes of the methylene asymmetric 2919 cm^{-1} peak is unreliable. We remove spectral interference of the base monolayer by depositing a perdeuterated dodecanethiolate (D12) monolayer, with the assumption that the chemistry of D12 film exchange is the same as that of a C12 monolayer. Unlike our STM measurements, alkyl chains of identical length are employed to simplify interpretation of the kinetics. The IR spectrum of a D12 monolayer can be found in the Supporting Information, Figure S2.

Figure 2A,B show the progression of the exchange reaction between a spectroscopically transparent D12 monolayer exposed to ethanolic C12Se. The C−H peaks of the C12Se film emerge with increasing exposure time, and the reaction terminates after complete D12 monolayer displacement. The relative ratio of peak intensities remains largely static throughout the displacement process, which implies that there is little reorganization during displacement (for example, we see no evidence of a transition between lying-down and standing-up phases,[86] as might be observed for deposition onto a bare substrate). Molecules are thus found in their near-final orientations shortly after incorporation into the film. Figure 2B shows the fractional coverage of C12Se monolayers versus immersion time. As can be seen in the STM images in Figure 3 (below), there is an initial phase of slower adsorption dominated by insertion at defect sites, followed by a period of more rapid replacement, and the rate ultimately slows as the reaction approaches completion. The predominant source of

error is sample-to-sample variability. Each gold substrate has a characteristic (and unquantified) fraction of steps and defects.[57,87] As the exchange reaction is initiated by insertion at defect sites, subtle differences in sample defect density can have large cumulative effects on the final rate of exchange. These differences are reflected in the standard deviation of fractional coverage at each time point.

The Johnson, Mehl, Avrami, and Kolmogorov (JMAK) model was devised originally to describe phase transitions in metal alloys.[88–90] We have previously used the site-saturated nucleation JMAK2 model to describe perimeter-dependent island growth of 1-adamantanethiolate exchange by C12, given as

$$\theta(t) = 1 - e^{(\kappa t)^2}$$

where κ is the rate constant.[57] Recent reports suggest that this model can be used generally to describe 2D film exchange.[91] For comparison, the kinetic data are fit to a variety of other models, including pure diffusion, first, second, and diffusion-limited Langmuir models, and the constant nucleation rate JMAK3 model. The JMAK2 model, used to fit the kinetic data in Figure 2B, best represents the data and is consistent with our observations of the reaction progression (a slower initial rate followed by a more rapid rate as coverage increased). As shown in Figure 2C, plotting the displacement rate versus the concentration of C12Se on a logarithmic scale gives a slope of ∼1, implying that the rate is directly proportional to the concentration of C12Se.

At nearly all conditions investigated, we observe that alkanethiolate monolayers are unstable in the presence of alkaneselenols. Co-deposition results in single-component C12Se monolayers, until the molar ratio approaches 100:1 in favor of the C12. Figure 2D shows the sharp transition between full-coverage C12Se and D12 monolayers as a function of mole fraction. In their work on benzenethiolates and selenolates, Huang et al. linked the faster kinetic exchange of benzenethiol and benzeneselenol to the pK_a of the selenol, suggesting that the deprotonated forms of the selenols were responsible for the faster exchange kinetics.[38] Our results examining the effect of solution pH on alkanethiolate displacement by selenol corroborate this finding: C12Se exchange with C10 SAMs was faster after addition of aqueous sodium hydroxide to the ethanolic selenolate solution. It remains unclear whether this increase in exchange rate is due primarily to deprotonation of the replacing species, or whether the hydroxide is facilitating abstraction of molecules from the preexisting monolayer. In all cases of hydroxide-catalyzed exchange, the methylene asymmetric stretch is observed to increase in intensity by a factor of 2–3 and shift from ∼2919 to ∼2930 cm^{-1}, indicative of poor order in the resulting film.[57,84] Annealing the film in the same solution at an elevated temperature for 24 h and then repeating the spectroscopic analysis reveals a monolayer film indistinguishable from one deposited at room temperature, evidence of poor ordering after base-catalyzed displacement of thiolate by selenolate. Spectra and kinetic results are collected in the Supporting Information, Figure S3.

Molecular Exchange of Decanethiolate by Dodecaneselenol. A preformed C10 SAM is exposed to 10 mM ethanolic C12Se for 1 min. The STM images in Figure 3A,A′ reveal rapid insertion of C12Se into the C10 lattice, notably at domain boundaries and at step-edges. The selenolates appear to occupy hexagonal lattices and to incorporate commensurately
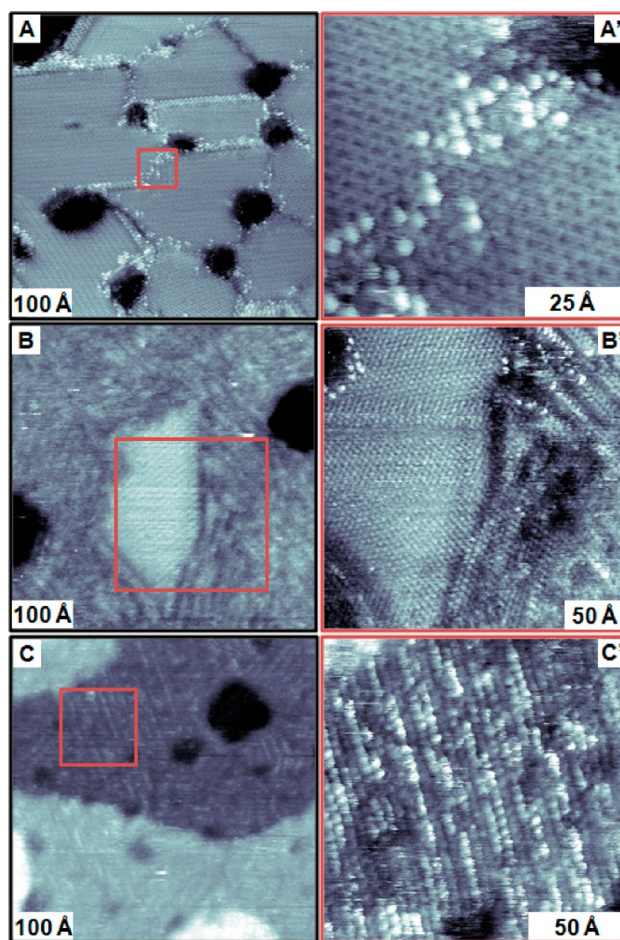

Figure 3. Scanning tunneling micrographs of mixed thiolate/selenolate self-assembled monolayers (SAMs) on Au{111}, all obtained at −1 V sample bias and 1 pA tunneling current. (A,A′) Brief exposure (1 min) of a C10 SAM to an ethanolic solution of 10 mM 1-dodecaneselenol (C12Se) results in adsorption at defect sites (step-edges and domain boundaries). The C12Se molecules appear to protrude from the C10 lattice by ∼0.7 Å in STM images. (B,B′) Longer exposure (4 min) resulted in substantial molecular exchange with C12Se, replacing C10 under these conditions. The relative apparent heights of the two species have reversed; the thiolates appear to protrude from the predominantly C12Se lattice by ∼0.7 Å in STM images. In B′, features at three different apparent heights can be observed in a single image; C12Se molecules (top left) appear to protrude from the C10 island by ∼0.7 Å, while the island appears ∼0.7 Å more protruding than nearby striped C12Se. Some intercalation of C10 within the C12Se striped phase cannot be excluded. (C,C′) After 10 min of exposure, no C10 molecules are observed, leaving only a striped phase of single-component C12Se.

to the lattices of the surrounding thiolates (Figure 3A′). Insertion has also been noted at isolated locations within ordered domains, likely a result of C12Se insertion at molecular vacancy defect sites (an example image is shown in the Supporting Information, Figure S1).

In these and most STM images, C12Se molecules appear to protrude somewhat more, here ∼0.7 Å, than the neighboring C10 molecules. The measured apparent height is related to the configuration of the STM tip, through which the tunneling current passes. We note that changes in the tip state result in variations of the observed relative apparent height. In some cases, inversion of the relative selenolate and thiolate conductance occurs after a change in the electronic properties
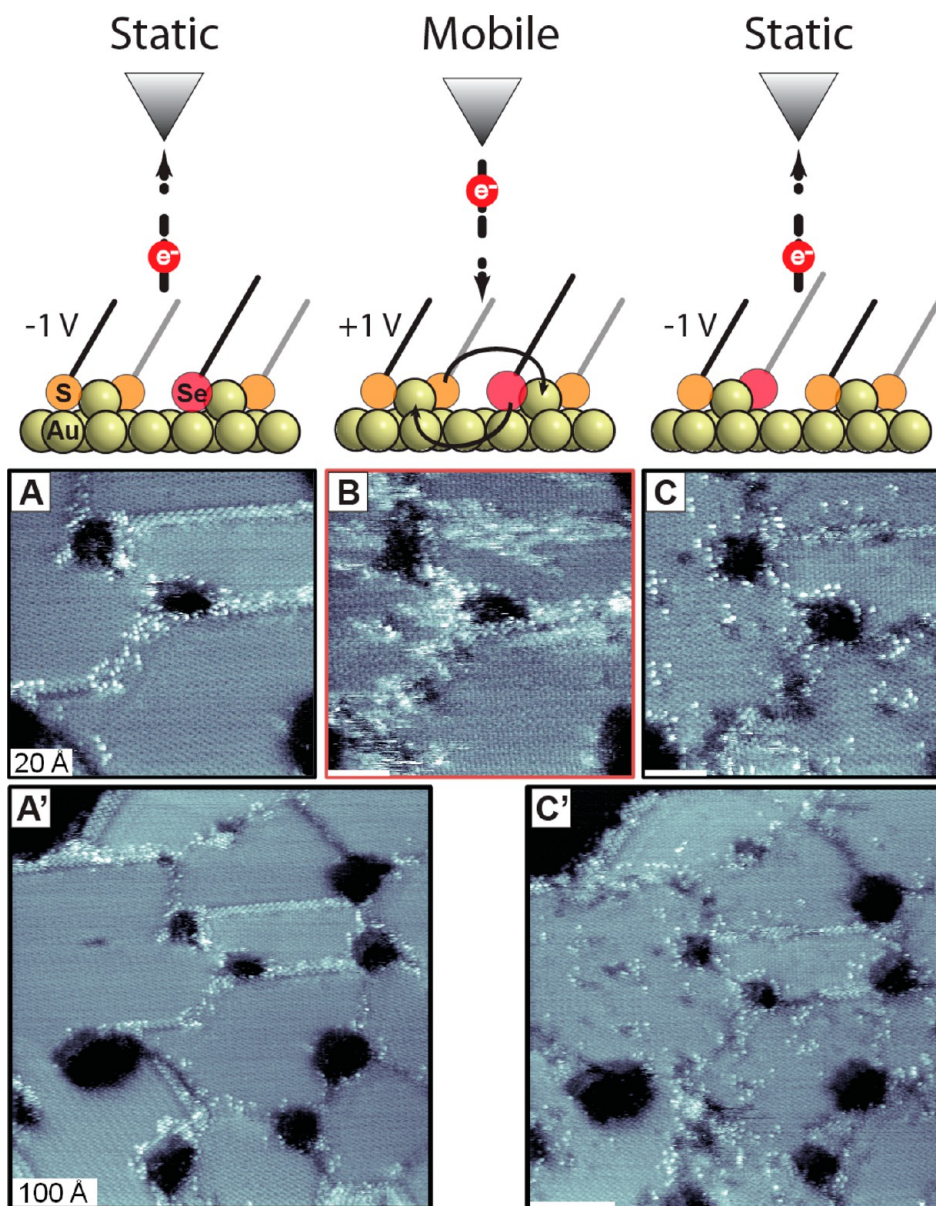
Figure 4. (Top) Schematic depicting direction of electron flow, sample bias, and reaction occurring between the gold (yellow circles) complex of selenolates (red circles), and thiolates (orange circles). Alkyl chains are denoted by black or gray lines. (Bottom) Sequence of images showing the effect of induced motion of 1-dodecaneselenolate (C12Se) in a 1-decanethiolate (C10) self-assembled monolayer. (A,A′) Scanning tunneling micrographs of C12Se molecules (appear protruding) inserted predominantly at step-edges and domain boundaries. Images were collected at −1 V sample bias and 3 pA tunneling current. (B) Image of the same region after reversal of the sample bias to +1 V. The reversal of bias polarity induces motion that enables C12Se to exchange positions with neighboring C10. The place-exchange reaction occurs faster than image acquisition, so the STM probe is no longer able to record the precise position of the selenolates.[103,104] (C,C′) Returning to −1 V sample bias halts the tip-induced motion of selenolates. Protruding molecules are observed in ordered C10 domains, having diffused several nanometers while the region was imaged at +1 V sample bias. The larger scan area, image C′, reveals that the motion of C12Se is induced at distances up to 50 nm from the tip position.

of the probe. This tendency for tip-dependent conductance changes must be carefully monitored to ensure that probe variations are distinguished from changes in molecular binding site. Examples of conductance reversal on tip state changes are shown in the Supporting Information, Figure S1.

Additional exposure to solution results in rapid increases in the relative C12Se coverages, with each site of C12Se insertion becoming a nucleation site for C12Se island growth.[57] After 4 min of C12Se exposure, C12Se is no longer confined to the regions in close proximity to C10 defect sites; it now occupies a substantial fraction of the surface. The relative apparent heights have inverted, with C12Se now appearing less protruding.

Ordered islands are the dominant configuration of the residual C10. Such large thiolate islands (appearing as the protruding features in Figure 3B,B′) have edge lengths of 100−500 Å. The largest, most ordered SAM domains are similarly most resistant to molecular exchange, as there are few internal defects to provide initiation sites for selenolate displacement, requiring molecular exchange to occur from the domain edges inward.

The displacement reaction does not appear to be a smooth progression between continuous domains of C10 to C12Se. The images in Figure 3C,C′ reveal striped features of high- and low-conductance rows. Comparing apparent heights of the striped regions, they are composed of features that match the

relative height of thiolate islands separated by less-protruding features. We attribute the greater protrusion of the features to structures at least partially composed of residual C10. We use apparent height as the marker for chemical identification. Low-coverage, inserted C12Se appears more protruding than C10 in STM images, while the striped features are equal to or lower in apparent height than C10. As the IR analysis suggests no change in absolute molecular coverage, these lower-height features are consistent with a different bonding configuration of the C12Se as relative coverage increases. The reaction progresses with incoming selenolates dismantling the organized domains of the C10 film, making coalescence into a single-component C12Se film rapid. This process appears to be anisotropic, with displacement favoring the direction along the rows rather than perpendicular to them.

Unlike the low-coverage example, the C12Se-dominated regions now appear less protruding than the C10 matrix. Figure 3B′ provides further evidence that the relative conductance of thiolates and selenolates is strongly influenced by the underlying substrate binding site. The image shows selenolates in two distinct conductance configurations: at the top left are selenolates that appear to protrude and are lattice matched to the C10, and on the right is the striped selenolate domain, which appears less protruding than the C10 island.

The apparent height of C12Se is observed to depend on the binding site. As mentioned previously, selenolates inserted at defects appear protruding from and lattice matched to the C10 lattice, which adopts a $(\sqrt{3} \times \sqrt{3})R30°$ lattice (and related superstructures). After the selenolates collapse into their own preferred bonding configuration, the alkanethiolate islands appear to protrude in STM images from the surrounding alkaneselenolate lattice by ~0.7 Å (for the conditions shown), despite the longer chain length of the C12Se molecules. This measurement is in close agreement with our previously reported value for C12 inserted into a C12Se SAM, wherein C12 molecules in STM images appeared to protrude from preformed C12Se SAMs.[27]

After a 7 min exposure to a C12Se solution, all C10 molecules were replaced by C12Se. The monolayer is configured differently than the directly deposited C12Se SAM, but the variations in apparent height in STM images remain. The structure is primarily striped, as shown in Figure 3C,C′, reflecting the linear propagation of the displacement reaction. Like the single-component C12Se film, the difference between the most and least protruding molecules in STM images on single terraces is ~1 Å.

The integrity of the top layer of the gold substrate is preserved by the displacement reaction. No aforementioned "trench" vacancy islands are observed after the alkaneselenolates have occupied the substrate surface, and the vacancy islands that form after thiolate SAM assembly are preserved by the new monolayer. This observation provides evidence that vacancy island formation is tied directly to lifting the Au herringbone reconstruction at the initial stage of SAM formation, and thus no new vacancy islands can form after thiolate replacement by selenolate. Likewise, we do not observe adatom islands, as would be expected if thiolates were abstracted and gold adatoms left behind.[8,10] At the early stages of the displacement reaction, the longer C12Se molecules appear lattice matched to the C10. In such cases, they are trapped in the same binding configuration as the sulfur in the C10 SAM. Later, as coverage increases, the selenolates are no

longer confined to thiolate-like configurations and adopt their own preferred binding configurations.

Bias-Induced Place Exchange of Selenolates with Thiolates. Local SAM coverage, structure, and composition can be used to tailor physical and chemical properties at interfaces. Phase-separated molecules can be selectively moved and removed via electrochemistry, where domains having weaker intermolecular interactions desorb at lower potential.[92,93] The STM probe has long been used to manipulate atoms and molecules directly, and to perform nanoscale lithographic patterning.[94−99] At relatively high voltages (sample bias of +3 V), the STM tip can be used to pattern alkanethiolate monolayers.[100−102] We have observed that the threshold for induced motion of the selenolates is lower, with motion observed at low sample biases, e.g., +1 V, and that we are able to manipulate alkaneselenolates selectively. This may be related to the promiscuous binding of selenolates to Au (relative to thiolates).[26]

For imaging without perturbing the SAM, we use a sample bias of −1 V at a tunneling current of 3 pA. Imaging at a sample bias of +1 V induces physical reorganization of thiolate/selenolate mixed monolayers. After reorganization, the overall film order is retained. At high selenolate coverage, the effect becomes more dramatic: both thiolate and selenolate domains become disordered, and mottled configurations of high- and low-conductance domains are observed (images can be found in the Supporting Information, Figure S4).

In Figures 4A,A′, C12Se molecules appear protruding relative to the C10 lattice. Upon bias polarity reversal (to +1 V sample bias), the positions of individual C12Se molecules are no longer well defined, as shown in Figure 4B. We attribute this "noise" to molecular place-exchange reactions and motion occurring at time scales faster than imaging.[103−106] Each image is recorded over ~4 min by moving the tip in a raster pattern over the interface, with the tip encountering individual protruding molecules at many positions, rather than over a single, well-defined binding site. In Figure 4C, a return to −1 V sample bias halts the place-exchange reactions, and the selenolates are again at well-defined sites. There are approximately the same numbers of molecules visible in the recorded area before and after bias-induced shuffling. A change in the tip geometry after bias reversal resulted in faint "double tip" artifacts to the lower right of all high-aspect-ratio protrusions, giving the false impression that more C12Se molecules are present in Figure 4C,C′. Selenolates are now observed incorporated into the centers of ordered domains. While the overall domain structures before and after place-exchange reactions are nominally the same, the movement of molecules to the new sites results in increased disorder. Protruding C12Se molecules are thus accompanied by depressions in the C10 lattice that arise from the additional free space created by decreases in the local alkyl chain crystallinity. The structures of the C10 domain boundaries have likewise been reconfigured.

While bias-induced place-exchange reactions are localized, the reactions are not limited to the specific position of the tunneling junction. Figure 4C′ shows that the monolayer was reconfigured as far as 50 nm from the region imaged at +1 V substrate bias. The tip scanned only over a 250 Å × 250 Å region, but molecules have been shuffled over the 500 Å × 500 Å terrace. Additional images recorded at distances greater than 500 Å from the region of induced motion reveal no apparent molecular place exchange (see Supporting Information, Figure S5).
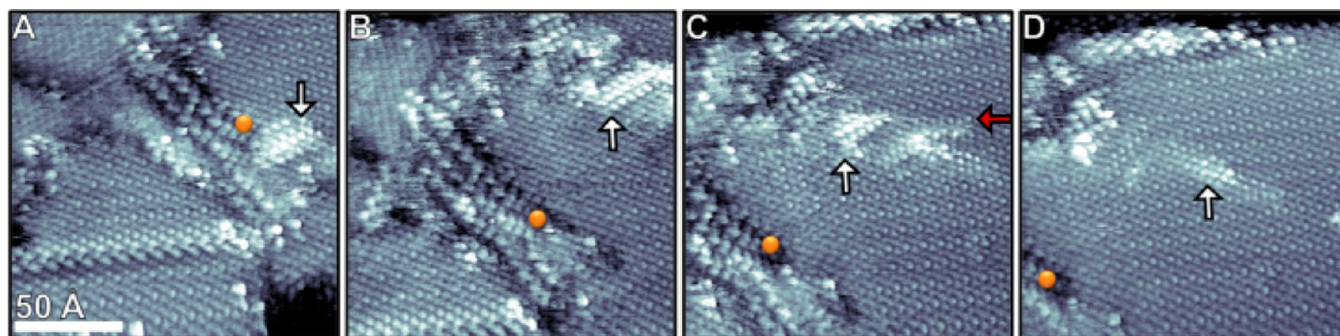
Figure 5. Application of a short voltage pulse over a C12Se cluster (+1 V sample bias, 3 pA, 5 s) induces 2D place-exchange reactions. Molecules that appear to protrude are attributed to 1-dodecaneselenolates in a 1-dodecanethiolate matrix. The pulse target, denoted by the orange circle, is labeled to account for drift over image acquisition times in excess of 5 min. The cluster denoted by the white arrow was the target of the voltage pulse. (B) In subsequent images, the cluster is displaced as a group and evolves over time. (C) The feature appears stable, and is then suddenly truncated at image line denoted in the red arrow, evidence of motion faster than the imaging time scale. (D) Subsequent images reveal continued changes in relative heights, with molecules likely drawn out of the field of view. The shift in image frame is because of drift over long image acquisition times (∼5 min/frame).

We demonstrated the ability to manipulate small groups of molecules with localized, short-duration voltage pulses, although the 500 Å range over which motion can be induced made directed assembly of individual molecules into specific patterns impractical. Figure 5 shows a small cluster of protruding C12Se molecules at which the STM tip is positioned. The sample bias is set to +1 V at 3 pA tunneling current for 5 s. Subsequent imaging at −1 V sample bias revealed substantial rearrangement of the local structure that continued long after the initial pulse. In many cases, however, short pulses had no obvious effects on the local structure at the scale imaged, but responses at distances larger than the imaging window could not be excluded. Evolution of the structure is observed to continue at faster than the minute time scale.

Implications for the Gold Adatom Complex. There is no evidence for the restructuring of the gold substrate during complete exchange reactions. C12Se SAMs deposited by displacement of C10 show evidence of the topographic variations characteristic of the selenolate system, but show vacancy islands characteristic of the C10 system (Figure 3C,C′). These features add to the existing evidence that the formation of vacancy islands is due to dynamics between the substrate and binding chalcogen as the herringbone reconstruction of the gold is lifted.[2,18,19,107] We conclude that the configuration of the gold–thiolate association is conserved after the initial molecular-exchange reaction, and additional reconfiguration that does not involve loss of gold atoms occurs as alkaneselenolate coverage increases.

Our observations support two distinct binding modes for selenolate on gold. In the early stages of the displacement reaction, C12Se molecules appear more protruding from the C10 lattice, and the apparent heights of the inserted C12Se are similar to the expected heights for C12 molecules inserted into C10 lattices. We postulate that the selenolates occupy the binding sites previously occupied by thiolates. Exchange at this early stage of the reaction is slow, and C12Se molecules are predominantly found at defects in the C10 SAM. In the later stages of the replacement reaction, the C12Se molecules appear lower than the C10 domains, and propagation of C12Se appears to occur in bands several molecules wide, with stripes of C10 remaining. We postulate that the gold–thiolate complexes exhibit long-range order in highly annealed films,

thus enabling linear stripes of selenolates to propagate over long distances (hundreds of Ångströms).

A barbell configuration of the gold adatom–thiolate complex has been proposed separately by several groups.[4,13,32,108,109] Several of our observations mesh well with this concept for the gold adatom complex. The early, high-conductance stage of C12Se insertion can be seen as an alkaneselenolate binding to and displacing the alkanethiolate from this complex, conserving the structure (Figure 3A,A′). As the coverage of selenolates increases, we note a change in structure and observed apparent heights of the selenolates (Figure 3B,B′). There are a number of mechanistic pathways that can explain the progression of the displacement mechanism. Thiolate desorption at SAM and substrate domain boundaries frees binding sites for selenol insertion from solution,[110] but does not account for the observed accelerated displacement after insertion.[20,57] A ligand-exchange model provides a mechanistic pathway for displacement, in which a selenolate binds at the thiolate-occupied complex adjacent to a defect site, and the thiolate is subsequently induced to desorb. This mechanism would require formation of a transient $Au(SeR)(SR)_2$ complex prior to desorption, which would likely not be observable at room temperature or at the slow experimental imaging time scales collected in this study.

It is less clear how to reconcile the barbell model with the mobility of the gold–selenolate complex and the patterns formed by the progression of the selenol–thiolate exchange reaction. Gold–thiolate complex mobility has long been an important concept for explaining the order and dynamics of alkanethiolate monolayers; however, the mobility we observe in the bias-induced reactions (as shown in Figure 4, above) is unprecedented. During the tip-induced place-exchange reactions, there are translation distances on the order of 5 nm (corresponding to a minimum of 10 molecular lattice site hops to reach the new location) for both individual and grouped C12Se. A turnstile mechanism relying on the transient trichalcogen gold complex described above is one possibility. If the selenolate dissociates from a complex and can hop to an adjacent complex after bias-induced activation, then the thiolate on the destination complex could, in turn, step back to effectively switch sites with the selenolate. Within the alkyl backbone superlattice and in the absence of available solution-phase interactions favoring abstraction, subsequent transfer of a

thiolate to the site vacated by the selenolate would be likely. The packing of the alkyl chains would be expected to deteriorate after repeated place exchanges by this mechanism, and this is observed as an increase in depressions in the monolayer (e.g., in comparison of panels A′ and C′ in Figure 5). As described above, at higher selenolate coverage, the mixed-monolayer system becomes randomly mixed, and order is lost after imaging at +1 V sample bias. Conversely, the gold adatom complexes may instead be swapping sites with neighbors, consistent with the observed mobility of the complex. Additional experiments and theoretical modeling will be required to address the question of the buried structure and mechanism of both molecular- and place-exchange reactions between thiolate/selenolate−gold complexes.

CONCLUSIONS AND PROSPECTS

Examining SAM molecular-exchange reactions through the lens of a gold adatom complex provides a variety of insights for interpreting the structural evolution from one complex supramolecular system to another, significantly less studied system. The atomic-scale configurations of gold−chalcogen bonds are deceptively complex. There are numerous phases of even simple alkanethiolates and alkaneselenolates on Au{111}.[26,86,111] We observed a monolayer transition from a full-coverage sulfur-bound C10 SAM to a full-coverage selenium-bound C12Se, taking note of how the gold substrate directs the progression of the reaction and the structures of the products.

In comparing single-component C10 and C12Se SAMs, there are numerous structural differences. We reported substrate vacancy trenches in single-component C12Se SAMs, which become visible as narrow, linear vacancy islands. These trenches are aligned with the close-packed substrate lattice directions. Likewise, the ±1 Å apparent height variations of highly ordered C12Se are grouped in similarly aligned substrate-matched patches and rows. The boundaries between groups of different apparent heights are less stark than the domain boundaries in ordered C10 domains. These observations are consistent with the viewpoints that there are more-varied binding sites available for selenolates and associated adatom complexes, and that apparent height is highly dependent on the Au−Se attachment geometry.

The molecular exchange of C10 by C12Se does not generate new vacancy trench features or adatom islands, suggesting that there is no ejection or reconstruction on thiolate replacement by selenium, pointing to conservation of the adatom complex (or of any other hypothesized motif) immediately following the exchange reaction. The contrast between the linear propagation of the thiolate/selenol displacement and the more radial growth mechanism of 1-adamantanethiolate displacement by alkanethiols may provide insight into the stoichiometry of the complexes involved and into mechanistic details of exchange at adatom complexes. The displacement reaction follows the JMAK2 site-saturated island growth mechanism, consistent with similar monolayer-exchange reactions.

We have observed that access to the substrate is required to initiate the exchange reaction, since insertion is observed predominantly at monolayer and substrate defect sites, and the insertion of a single molecule creates an adjacent molecular defect site. Also, inserted C12Se molecules appear lattice-matched to adjacent C10 molecules due to molecule−molecule interactions. For low-fraction C12Se monolayers, we conclude that the selenolates have adopted thiolate-like binding

configurations with the gold substrate, and as coverage is increased, the disruption of ordered alkanethiolate domains appears to occur directionally. From this result, we infer that the adatom layer is ordered in the highly annealed C10 films we employ. Multiple binding configurations have been shown previously to be close energetically, indicating that there are multiple stable possibilities for substrate attachment. The low-energy barbell configuration may be consistent with these results; however, future experiments with grazing-angle X-ray diffraction and local barrier height imaging[50] will be necessary to elucidate binding configurations of C12Se and C12S. The data shown will have implications not only for the Au−S bond complexes, but also in the field of chemical patterning down to the single-molecule scale.[87]

Finally, we also observed a low (≤1 eV) barrier to induced motion of C12Se by the STM tip at positive sample bias, where electrons injected into empty states of the mixed-monolayer film induce place-exchange reactions between the selenolates and thiolates. During motion, adjacent sites seem to have equal probability of providing a new attachment site, assuming the substrate bond configuration is the same. The atomistic nature of this reaction remains an open question. We postulate that application of positive sample bias induces a local thiolate-to-selenolate ligand-exchange metathesis reaction between adjacent gold adatom complexes. A turnstile adatom trichalcogen transitional state would account for the capacity of isolated selenolates to move through an ordered lattice without inducing extensive monolayer order.

MATERIALS AND METHODS

1-Dodecaneselenol was prepared by reduction of di(dodecyl)-diselenide with LiAlH₄ in diethyl ether. After an acidic work-up, the product was purified by distillation over a 30 cm Vigreux column at a pressure of 20 hPa. It is vital to strictly exclude oxygen throughout each preparation step. 1-Decanethiol, 1-dodecanethiol, and absolute ethanol (non-denatured) were used as received from Sigma-Aldrich (St. Louis, MO). Perdeuterated 1-dodecanethiol was used as received from CDN Isotopes (Canada). For air-sensitive work, ethanol is degassed via freeze−pump−thaw cycles as described previously,[32] and is subsequently transferred to a sealed, gasketed bottle stored inside an oxygen-free (<1 ppm) glovebox. All glassware was cleaned by immersion in fresh piranha solution (1:3 H₂O₂ and concentrated sulfuric acid) and thorough rinsing in deionized water supplied by a Milli-Q system from Millipore (Billerica, MA). *Caution! These solutions are strongly acidic and oxidizing, reactions are energetic, and improper use or disposal could result in explosion or severe burns.*

Preparation of Substrates and Self-Assembled Monolayers. Gold-on-mica substrates (Agilent, Santa Clara, CA) and gold-on-silicon (prepared by electron beam evaporation of 1000 Å Au on a 50 Å Cr adhesion layer, without breaking vacuum, at a rate of 1 Å s⁻¹ onto a *p*-type silicon wafer supplied by Silicon Quest International, Santa Clara, CA) are annealed by 40 passes of a hydrogen flame at an approximate rate of 0.5 Hz. *Caution! Use appropriate engineering controls when striking a flame from a compressed fuel cylinder.* The flame is struck from a quartz tip, which is held at a 45° angle while being passed over the substrate. Substrates for C12 SAM fabrication are used immediately after preparation, and the time between annealing and C12Se fabrication is minimized. Titanium adhesion layers for gold substrates are not recommended, as the metal can peel from the substrate in response to flame exposure.

Preparation of exceptionally well-ordered, stable SAMs is achieved through control of deposition conditions. The C10, C12, and D12 solutions are prepared by transferring the appropriate volume of neat liquid substance to a volumetric flask, the mass confirmed gravimetrically. Flasks are then filled to the appropriate volume with ethanol. A freshly flame-annealed substrate is quickly immersed in the solution.

Since full monolayer coverage is achieved within milliseconds of solution contact, excess volume is withdrawn. The gold substrate is left exposed to the airspace in the vial over a small volume of residual solution. The vial is capped and placed in a furnace set to 78 °C for a minimum of 24 h and up to 5 days. Under these vapor annealing conditions, SAM domain sizes grow exceptionally large, and the SAM is well ordered, conditions conducive to imaging substrate-linked structures through minimization of alkyl backbone orientational defects. Any oxidative degradation of the film is immediately healed, maintaining film quality indefinitely until just before imaging or further modification. These well-ordered films resist oxidative degradation better than films deposited rapidly or at room temperature, and thus support stable continuous imaging for several days.

C12Se solutions are prepared in an oxygen- and water-free glovebox. Organic thiols and selenols can contaminate a glovebox environment, so care is taken to minimize clean substrate exposure to the glovebox environment. Sample transfer operations are thus conducted rapidly, typically less than 3 s. Two vials are each filled with 1 mL of ethanol degassed via freeze−pump−thaw cycles. The first vial is kept sealed, and is held in reserve for a later rinsing step. One microliter of C12Se is added to the first vial. A 5 min purge procedure is then performed on the glovebox environment. A freshly annealed substrate is placed in a gasketed vial, which has been briefly purged with a stream of nitrogen prior to sealing. The sample is then transferred to the glovebox, removed from the vial, and quickly immersed in the C12Se solution for 24 h. At the end of the immersion, the sample is removed from C12Se solution and placed immediately into the vial of neat ethanol, which is removed from the glovebox. The film, which is not air sensitive, is then rinsed with neat ethanol and dried with nitrogen.

For molecular-exchange experiments, the prefabricated initial sample is placed in a solution of the specified concentration for the specified time. Exchange by C12Se is performed inside the environmental glovebox, and exchange by C10, C12, or D12 is performed under atmospheric conditions.

Scanning Tunneling Microscopy Measurements. All images were collected on a custom-built beetle-style STM in atmospheric air and at room temperature, as described previously.[112] The Pt/Ir 90:10 tip wire was supplied by Alfa Aesar (Ward Hill, MA). The gain of the piezoelectric scanners was calibrated by comparison of a C10 monolayer on Au{111} to its known lattice constant of 4.99 Å. To ensure low drift, the STM tip is held in tunneling for as long as several days. Imaging of C12Se films is highly dependent on the state of the tip, which can change during imaging. Values reported were for stable and reproducible tips that could generally persist for several days. If a tip changed states frequently, a new tip was either cut immediately, or the instrument was left in tunneling for a period of several hours.

Infrared Reflectance Absorption Spectroscopy Measurements. All IR spectra were collected on a Nicolet 8700 equipped with a Seagull variable angle reflection accessory, supplied by Harrick Scientific, Inc. (Ossining, NY). The spectrometer was purged by an FTIR purge gas generator supplied by Parker-Balston (Cleveland, OH). Each spectrum was the result of between 512 and 1024 multiplexed scans, obtained at the grazing incidence angle of 84° relative to sample normal, and at a resolution of 4 cm^{-1}. For fractional coverage determination, samples were held in 1 mM exchange solution (typically ethanolic C12SeH) for 24 h to provide a 100% selenate coverage substrate having reflective properties identical to those used for the kinetic experiment. Consequently, absolute coverage in the kinetic experiment increases slightly in that time. This small source of systematic error results in the observed kinetic trend of sub-100% maximum within the kinetic experimental time scale.

ASSOCIATED CONTENT

Ⓢ Supporting Information

Additional STM images of C12Se and C12Se/C12 SAMs emphasizing conductance reversal on tip state changes; spectroscopic data related to effect of pH on exchange kinetics; images of film disorder induced in selenolate-rich mixed SAMs at positive sample bias; additional images of tip-induced motion in selenolate-poor SAMs. This material is available free of charge via the Internet at http://pubs.acs.org.

AUTHOR INFORMATION

Corresponding Authors
hohmanjn@stanford.edu
aterfort@chemie.uni-frankfurt.de
psw@cnsi.ucla.edu

Notes
The authors declare no competing financial interest.

REFERENCES

(1) Stranick, S. J.; Parikh, A. N.; Allara, D. L.; Weiss, P. S. *J. Phys. Chem.* **1994**, *98*, 11136−11142.
(2) Maksymovych, P.; Sorescu, D. C.; Yates, J. T. *Phys. Rev. Lett.* **2006**, *97*, 146103.
(3) Yu, M.; Bovet, N.; Satterley, C. J.; Bengio, S.; Lovelock, K. R. J.; Milligan, P. K.; Jones, R. G.; Woodruff, D. P.; Dhanak, V. *Phys. Rev. Lett.* **2006**, *97*, 166102.
(4) Jadzinsky, P. D.; Calero, G.; Ackerson, C. J.; Bushnell, D. A.; Kornberg, R. D. *Science* **2007**, *318*, 430−433.
(5) Mazzarello, R.; Cossaro, A.; Verdini, A.; Rousseau, R.; Casalis, L.; Danisman, M. F.; Floreano, L.; Scandolo, S.; Morgante, A.; Scoles, G. *Phys. Rev. Lett.* **2007**, *98*, 4.
(6) Maksymovych, P.; Yates, J. T. *J. Am. Chem. Soc.* **2008**, *130*, 7518−7519.
(7) Cossaro, A.; Mazzarello, R.; Rousseau, R.; Casalis, L.; Verdini, A.; Kohlmeyer, A.; Floreano, L.; Scandolo, S.; Morgante, A.; Klein, M. L.; Scoles, G. *Science* **2008**, *321*, 943−946.
(8) Kautz, N. A.; Kandel, S. A. *J. Am. Chem. Soc.* **2008**, *130*, 6908−6909.
(9) Voznyy, O.; Dubowski, J. J.; Yates, J. T.; Maksymovych, P. *J. Am. Chem. Soc.* **2009**, *131*, 12989−12993.
(10) Kautz, N. A.; Kandel, S. A. *J. Phys. Chem. C* **2009**, *113*, 19286−19291.
(11) Qian, H.; Eckenhoff, W. T.; Zhu, Y.; Pintauer, T.; Jin, R. *J. Am. Chem. Soc.* **2010**, *132*, 8280−8281.
(12) Liu, Y.; Ozolins, V. *J. Phys. Chem. C* **2012**, *116*, 4738−4747.
(13) Hakkinen, H. *Nat. Chem.* **2012**, *4*, 443−455.
(14) Knoppe, S.; Dolamic, I.; Bürgi, T. *J. Am. Chem. Soc.* **2012**, *134*, 13114−13120.
(15) Fan, X.; Zhang, C.; Liu, Y.; Lau, W. M. *J. Phys. Chem. C* **2012**, *116*, 19909−19917.
(16) Moore, A. M.; Mantooth, B. A.; Donhauser, Z. J.; Yao, Y. X.; Tour, J. M.; Weiss, P. S. *J. Am. Chem. Soc.* **2007**, *129*, 10352−10353.
(17) Poirier, G. E. *Langmuir* **1997**, *13*, 2019−2026.
(18) Akihiro, N.; Yoshitada, M. *J. Phys.: Condens. Matter* **2007**, *19*, 365245.
(19) Jewell, A. D.; Tierney, H. L.; Sykes, E. C. H. *Phys. Rev. B* **2010**, *82*, 205401.
(20) Schlenoff, J. B.; Li, M.; Ly, H. *J. Am. Chem. Soc.* **1995**, *117*, 12528−12536.
(21) Shon, Y. S.; Lee, T. R. *J. Phys. Chem. B* **2000**, *104*, 8192−8200.
(22) Moore, A. M.; Mantooth, B. A.; Donhauser, Z. J.; Maya, F.; Price, D. W.; Yao, Y. X.; Tour, J. M.; Weiss, P. S. *Nano Lett.* **2005**, *5*, 2292−2297.

(23) Kassam, A.; Bremner, G.; Clark, B.; Ulibarri, G.; Lennox, R. B. *J. Am. Chem. Soc.* **2006**, *128*, 3476−3477.

(24) Patole, S. N.; Baddeley, C. J.; O'Hagan, D.; Richardson, N. V. *J. Phys. Chem. C* **2008**, *112*, 13997−14000.

(25) Ballav, N.; Terfort, A.; Zharnikov, M. *J. Phys. Chem. C* **2009**, *113*, 3697−3706.

(26) Monnell, J. D.; Stapleton, J. J.; Jackiw, J. J.; Dunbar, T.; Reinerth, W. A.; Dirk, S. M.; Tour, J. M.; Allara, D. L.; Weiss, P. S. *J. Phys. Chem. B* **2004**, *108*, 9834−9841.

(27) Monnell, J. D.; Stapleton, J. J.; Dirk, S. M.; Reinerth, W. A.; Tour, J. M.; Allara, D. L.; Weiss, P. S. *J. Phys. Chem. B* **2005**, *109*, 20343−20349.

(28) Bashir, A.; Käfer, D.; Müller, J.; Wöll, C.; Terfort, A.; Witte, G. *Angew. Chem., Int. Ed.* **2008**, *47*, 5250−5252.

(29) Cyganik, P.; Szelagowska-Kunstman, K.; Terfort, A.; Zharnikov, M. *J. Phys. Chem. C* **2008**, *112*, 15466−15473.

(30) Track, A. M.; Rissner, F.; Heimel, G.; Romaner, L.; Käfer, D.; Bashir, A.; Rangger, G. M.; Hofmann, O. T.; Bucko, T.; Witte, G.; Zojer, E. *J. Phys. Chem. C* **2010**, *114*, 2677−2684.

(31) Weidner, T.; Ballav, N.; Grunze, M.; Terfort, A.; Zharnikov, M. *Phys. Status Solidi B* **2009**, *246*, 1519−1528.

(32) Hohman, J. N.; Kim, M.; Schüpbach, B.; Kind, M.; Thomas, J. C.; Terfort, A.; Weiss, P. S. *J. Am. Chem. Soc.* **2011**, *133*, 19422−19431.

(33) Yokota, K.; Taniguchi, M.; Tsutsui, M.; Kawai, T. *J. Am. Chem. Soc.* **2011**, *132*, 17364−17365.

(34) Cometto, F. P.; Patrito, E. M.; Paredes Olivera, P.; Zampieri, G.; Ascolani, H. *Langmuir* **2012**, *28*, 13624−13635.

(35) Kurashige, W.; Yamaguchi, M.; Nobusada, K.; Negishi, Y. *J. Phys. Chem. Lett.* **2012**, *3*, 2649−2652.

(36) Pathem, B. K.; Claridge, S. A.; Zheng, Y. B.; Weiss, P. S. *Annu. Rev. Phys. Chem.* **2013**, *64*, 605−630.

(37) Romashov, L. V.; Ananikov, V. P. *Chem.—Eur. J.* **2013**, *19*, 17640−17660.

(38) Huang, F. K.; Horton, R. C.; Myles, D. C.; Garrell, R. L. *Langmuir* **1998**, *14*, 4802−4808.

(39) Szelągowska-Kunstman, K.; Cyganik, P.; Schüpbach, B.; Terfort, A. *Phys. Chem. Chem. Phys.* **2010**, *12*, 4400−4406.

(40) Stipe, B. C.; Rezaei, M. A.; Ho, W. *Science* **1998**, *280*, 1732−1735.

(41) Bumm, L. A.; Arnold, J. J.; Dunbar, T. D.; Allara, D. L.; Weiss, P. S. *J. Phys. Chem. B* **1999**, *103*, 8122−8127.

(42) Weiss, P. S.; Eigler, D. M. *Phys. Rev. Lett.* **1993**, *71*, 3139−3142.

(43) Donhauser, Z. J.; Mantooth, B. A.; Kelly, K. F.; Bumm, L. A.; Monnell, J. D.; Stapleton, J. J.; Price, D. W.; Rawlett, A. M.; Allara, D. L.; Tour, J. M.; Weiss, P. S. *Science* **2001**, *292*, 2303−2307.

(44) Camillone, N.; Eisenberger, P.; Leung, T. Y. B.; Schwartz, P.; Scoles, G.; Poirier, G. E.; Tarlov, M. J. *J. Chem. Phys.* **1994**, *101*, 11031−11036.

(45) Poirier, G. E.; Tarlov, M. J. *Langmuir* **1994**, *10*, 2853−2856.

(46) Poirier, G. E. *Chem. Rev.* **1997**, *97*, 1117−1127.

(47) Weiss, P. S. *Acc. Chem. Res.* **2008**, *41*, 1772−1781.

(48) Love, J. C.; Estroff, L. A.; Kriebel, J. K.; Nuzzo, R. G.; Whitesides, G. M. *Chem. Rev.* **2005**, *105*, 1103−1169.

(49) Bent, S. F. *ACS Nano* **2007**, *1*, 10−12.

(50) Han, P.; Kurland, A. R.; Giordano, A. N.; Nanayakkara, S. U.; Blake, M. M.; Pochas, C. M.; Weiss, P. S. *ACS Nano* **2009**, *3*, 3115−3121.

(51) Choi, J.; Lee, Y. J.; Kang, H.; Han, J. W.; Noh, J. *Bull. Korean Chem. Soc.* **2008**, *29*, 1229−1232.

(52) Yang, G.; Liu, G.-y. *J. Phys. Chem. B* **2003**, *107*, 8746−8759.

(53) de la Llave, E.; Scherlis, D. A. *Langmuir* **2010**, *26*, 173−178.

(54) Dameron, A. A.; Charles, L. F.; Weiss, P. S. *J. Am. Chem. Soc.* **2005**, *127*, 8697−8704.

(55) Dameron, A. A.; Mullen, T. J.; Hengstebeck, R. W.; Saavedra, H. M.; Weiss, P. S. *J. Phys. Chem. C* **2007**, *111*, 6747−6752.

(56) Mullen, T. J.; Dameron, A. A.; Saavedra, H. M.; Williams, M. E.; Weiss, P. S. *J. Phys. Chem. C* **2007**, *111*, 6740−6746.

(57) Saavedra, H. M.; Barbu, C. M.; Dameron, A. A.; Mullen, T. J.; Crespi, V. H.; Weiss, P. S. *J. Am. Chem. Soc.* **2007**, *129*, 10741−10746.

(58) Bumm, L. A.; Arnold, J. J.; Cygan, M. T.; Dunbar, T. D.; Burgin, T. P.; Jones, L.; Allara, D. L.; Tour, J. M.; Weiss, P. S. *Science* **1996**, *271*, 1705−1707.

(59) Cygan, M. T.; Dunbar, T. D.; Arnold, J. J.; Bumm, L. A.; Shedlock, N. F.; Burgin, T. P.; Jones, L.; Allara, D. L.; Tour, J. M.; Weiss, P. S. *J. Am. Chem. Soc.* **1998**, *120*, 2721−2732.

(60) Donhauser, Z. J.; Price, D. W.; Tour, J. M.; Weiss, P. S. *J. Am. Chem. Soc.* **2003**, *125*, 11462−11463.

(61) Weck, M.; Jackiw, J. J.; Rossi, R. R.; Weiss, P. S.; Grubbs, R. H. *J. Am. Chem. Soc.* **1999**, *121*, 4088−4089.

(62) Kim, M.; Hohman, J. N.; Cao, Y.; Houk, K. N.; Ma, H.; Jen, A. K.-Y.; Weiss, P. S. *Science* **2011**, *331*, 1312−1315.

(63) Zheng, Y. B.; Pathem, B. K.; Hohman, J. N.; Thomas, J. C.; Kim, M.; Weiss, P. S. *Adv. Mater.* **2013**, *25*, 293−293.

(64) Poirier, G. E.; Tarlov, M. J.; Rushmeier, H. E. *Langmuir* **1994**, *10*, 3383−3386.

(65) Dishner, M. H.; Feher, F. J.; Hemminger, J. C. *Chem. Commun.* **1996**, 1971−1972.

(66) Smith, R. K.; Lewis, P. A.; Weiss, P. S. *Prog. Surf. Sci.* **2004**, *75*, 1−68.

(67) Yang, G.; Amro, N. A.; Starkewolfe, Z. B.; Liu, G.-y. *Langmuir* **2004**, *20*, 3995−4003.

(68) Stranick, S. J.; Parikh, A. N.; Allara, D. L.; Weiss, P. S. *J. Phys. Chem.* **1994**, *98*, 11136−11142.

(69) Kim, M.; Hohman, J. N.; Morin, E. I.; Daniel, T. A.; Weiss, P. S. *J. Phys. Chem. A* **2009**, *113*, 3895−3903.

(70) Saavedra, H. M.; Thompson, C. M.; Hohman, J. N.; Crespi, V. H.; Weiss, P. S. *J. Am. Chem. Soc.* **2009**, *131*, 2252−2259.

(71) Saavedra, H. M.; Mullen, T. J.; Zhang, P. P.; Dewey, D. C.; Claridge, S. A.; Weiss, P. S. *Rep. Prog. Phys.* **2010**, *73*, 036501.

(72) Shaporenko, A.; Ulman, A.; Terfort, A.; Zharnikov, M. *J. Phys. Chem. B* **2005**, *109*, 3898−3906.

(73) Yee, C. K.; Ulman, A.; Ruiz, J. D.; Parikh, A.; White, H.; Rafailovich, M. *Langmuir* **2003**, *19*, 9450−9458.

(74) Fonder, G.; Cecchet, F.; Peremans, A.; Thiry, P. A.; Delhalle, J.; Mekhalif, Z. *Surf. Sci.* **2009**, *603*, 2276−2282.

(75) Fonder, G.; Delhalle, J.; Mekhalif, Z. *Appl. Surf. Sci.* **2011**, *256*, 2968−2973.

(76) Aizenberg, J.; Black, A. J.; Whitesides, G. M. *Nature* **1998**, *394*, 868.

(77) Black, A. J.; Paul, K. E.; Aizenberg, J.; Whitesides, G. M. *J. Am. Chem. Soc.* **1999**, *121*, 8356−8365.

(78) Collard, D. M.; Fox, M. A. *Langmuir* **1991**, *7*, 1192−1197.

(79) Baralia, G. G.; Duwez, A.-S.; Nysten, B.; Jonas, A. M. *Langmuir* **2005**, *21*, 6825−6829.

(80) Hohman, J. N.; Claridge, S. A.; Kim, M.; Weiss, P. S. *Mater. Sci. Eng., R* **2010**, *70*, 188−208.

(81) Kamenetska, M.; Quek, S. Y.; Whalley, A. C.; Steigerwald, M. L.; Choi, H. J.; Louie, S. G.; Nuckolls, C.; Hybertsen, M. S.; Neaton, J. B.; Venkataraman, L. *J. Am. Chem. Soc.* **2010**, *132*, 6817−6821.

(82) Hill, I. R.; Levin, I. W. *J. Chem. Phys.* **1979**, *70*, 842−851.

(83) Porter, M. D.; Bright, T. B.; Allara, D. L.; Chidsey, C. E. D. *J. Am. Chem. Soc.* **1987**, *109*, 3559−3568.

(84) Nuzzo, R. G.; Dubois, L. H.; Allara, D. L. *J. Am. Chem. Soc.* **1990**, *112*, 558−569.

(85) Choi, J.; Kang, H.; Ito, E.; Hara, M.; Noh, J. *Bull. Korean Chem. Soc.* **2011**, *32*, 2623−2627.

(86) Vericat, C.; Vela, M. E.; Salvarezza, R. C. *Phys. Chem. Chem. Phys.* **2005**, *7*, 3258−3268.

(87) Claridge, S. A.; Liao, W.-S.; Thomas, J. C.; Zhao, Y.; Cao, H. H.; Cheunkar, S.; Serino, A. C.; Andrews, A. M.; Weiss, P. S. *Chem. Soc. Rev.* **2012**, *42*, 2725−2745.

(88) Avrami, M. *J. Chem. Phys.* **1939**, *7*, 1103−1112.

(89) Avrami, M. *J. Chem. Phys.* **1940**, *8*, 212−224.

(90) Avrami, M. *J. Chem. Phys.* **1941**, *9*, 177−184.

(91) Wang, Y.; Zeiri, O.; Neyman, A.; Stellacci, F.; Weinstock, I. A. *ACS Nano* **2012**, *6*, 629−640.

(92) Hobara, D.; Sasaki, T.; Imabayashi, S.-i.; Kakiuchi, T. *Langmuir* **1999**, *15*, 5073−5078.

(93) Mullen, T. J.; Dameron, A. A.; Weiss, P. S. *J. Phys. Chem. B* **2006**, *110*, 14410−14417.

(94) Eigler, D. M.; Schweizer, E. K. *Nature* **1990**, *344*, 524−526.

(95) Avouris, P.; Lyo, I.-W.; Bozso, F. *J. Vac. Sci. Technol., B* **1991**, *9*, 424−430.

(96) Weiss, P. S.; Eigler, D. M. *Phys. Rev. Lett.* **1992**, *69*, 2240−2243.

(97) Lyding, J. W.; Hess, K.; Abeln, G. C.; Thompson, D. S.; Moore, J. S.; Hersam, M. C.; Foley, E. T.; Lee, J.; Chen, Z.; Hwang, S. T.; Choi, H.; Avouris, P.; Kizilyalli, I. C. *Appl. Surf. Sci.* **1998**, *130−132*, 221−230.

(98) Liu, M.; Amro, N. A.; Liu, G.-y. *Annu. Rev. Phys. Chem.* **2008**, *59*, 367−386.

(99) Luis, G. R.; Jian, L. *J. Phys.: Condens. Matter* **2009**, *21*, 483001.

(100) Liu, G.-y.; Xu, S.; Qian, Y. *Acc. Chem. Res.* **2000**, *33*, 457−466.

(101) Cheung, C. L.; Camarero, J. A.; Woods, B. W.; Lin, T. W.; Johnson, J. E.; De Yoreo, J. J. *J. Am. Chem. Soc.* **2003**, *125*, 6848−6849.

(102) Kramer, S.; Fuierer, R. R.; Gorman, C. B. *Chem. Rev.* **2003**, *103*, 4367−4418.

(103) Stranick, S. J.; Kamna, M. M.; Weiss, P. S. *Science* **1994**, *266*, 99−102.

(104) Mantooth, B. A.; Sykes, E. C. H.; Han, P.; Moore, A. M.; Donhauser, Z. J.; Crespi, V. H.; Weiss, P. S. *J. Phys. Chem. C* **2007**, *111*, 6167−6182.

(105) Claridge, S. A.; Schwartz, J. J.; Weiss, P. S. *ACS Nano* **2011**, *5*, 693−729.

(106) Tarr, S.; Weiss, P. S. *Leonardo* **2012**, *45*, 439−445.

(107) Nenchev, G.; Diaconescu, B.; Hagelberg, F.; Pohl, K. *Phys. Rev. B* **2009**, *80*, 081401.

(108) Zhu, M.; Aikens, C. M.; Hollander, F. J.; Schatz, G. C.; Jin, R. *J. Am. Chem. Soc.* **2008**, *130*, 5883−5885.

(109) Maksymovych, P.; Voznyy, O.; Dougherty, D. B.; Sorescu, D. C.; Yates, J. T. *Prog. Surf. Sci.* **2010**, *85*, 206−240.

(110) Lewis, P. A.; Donhauser, Z. J.; Mantooth, B. A.; Smith, R. K.; Bumm, L. A.; Kelly, K. F.; Weiss, P. S. *Nanotechnology* **2001**, *12*, 231−237.

(111) Qian, Y.; Yang, G.; Yu, J.; Jung, T. A.; Liu, G.-y. *Langmuir* **2003**, *19*, 6056−6065.

(112) Bumm, L. A.; Arnold, J. J.; Charles, L. F.; Dunbar, T. D.; Allara, D. L.; Weiss, P. S. *J. Am. Chem. Soc.* **1999**, *121*, 8017−8021.